© 2018. Published by The Company of Biologists Ltd | Development (2018) 145, dev163691. doi:10.1242/dev.163691

RESEARCH ARTICLE

Pax6 regulation of *Sox9* in the mouse retinal pigmented epithelium controls its timely differentiation and choroid vasculature development

Yamit Cohen-Tayar[1], Hadar Cohen[2], Yulia Mitiagin[3], Zohar Abravanel[1], Carmit Levy[1], Masha Idelson[4], Benjamin Reubinoff[4], Shalev Itzkovitz[5], Shaul Raviv[1], Klaus H. Kaestner[6], Pablo Blinder[3,7], Ran Elkon[1,7,*] and Ruth Ashery-Padan[1,7,*]

ABSTRACT

The synchronized differentiation of neuronal and vascular tissues is crucial for normal organ development and function, although there is limited information about the mechanisms regulating the coordinated development of these tissues. The choroid vasculature of the eye serves as the main blood supply to the metabolically active photoreceptors, and develops together with the retinal pigmented epithelium (RPE). Here, we describe a novel regulatory relationship between the RPE transcription factors Pax6 and Sox9 that controls the timing of RPE differentiation and the adjacent choroid maturation. We used a novel machine learning algorithm tool to analyze high resolution imaging of the choroid in *Pax6* and *Sox9* conditional mutant mice. Additional unbiased transcriptomic analyses in mutant mice and RPE cells generated from human embryonic stem cells, as well as chromatin immunoprecipitation and high-throughput analyses, revealed secreted factors that are regulated by Pax6 and Sox9. These factors might be involved in choroid development and in the pathogenesis of the common blinding disease: age-related macular degeneration (AMD).

KEY WORDS: Retinal pigmented epithelium, Pax6, Sox9, Choroid vasculature, Age-related macular degeneration

INTRODUCTION

Normal organogenesis requires the synchronized differentiation of multiple cell lineages. In recent years, we have gained extensive knowledge about the transcription factors (TFs) that control the fates of specific lineages; however, the mechanisms that control the timing of gene expression and synchronize the differentiation of adjacent tissues remain largely unknown. Moreover, despite the involvement of the retinal pigmented epithelium (RPE) and the choroid blood vessels in various retinal dystrophies, such as age-related macular degeneration (AMD) (Hageman et al., 2001) and retinitis pigmentosa (Wang et al., 2001), choroid development is poorly understood. Here, we describe a novel interplay between two key TFs that regulates the timely differentiation of the RPE and guides the development of the adjacent choroid vasculature.

The RPE is a monolayer of polarized pigmented epithelial cells, which comprise the retinal-blood barrier, and mediate the selective transport of ions, nutrients and water from the choroidal blood vessels to the outer retina (Strauss, 2005). The underlying choroid consists of four layers: Bruch's membrane, the choriocapillaris (CC), and the Sattler's and Haller's layers of medium-sized blood vessels (Hayreh, 1975; Nickla and Wallman, 2010). RPE differentiation takes place in conjunction with the development of neighboring tissues and is a gradual process. Like the development of the retina, RPE differentiation starts from the central cells, and progresses toward the optic cup periphery (Defoe and Levine, 2003). The RPE is known to play a crucial role during the development and maintenance of both the choroid and retinal photoreceptors (Amram et al., 2017), where RPE cells secrete growth factors, such as vascular endothelial growth factor (VEGF) (Blaauwgeers et al., 1999), that are important for choroid development (Marneros et al., 2005) and maintenance (Saint-Geniez et al., 2006). Interestingly, although the development of the choroidal blood vessels is parallel to the establishment of the RPE (Korte et al., 1984; Spilsbury et al., 2000; Zhao and Overbeek, 2001), the appearance of melanocytes, maturation of the choroidal layers and the development of Bruch's membrane are initiated only in late gestation (Lutty et al., 2010; Sellheyer, 1990). Hence, these processes could be guided by different factors expressed temporally during embryonic development.

Two factors implicated in the early or late stages of RPE differentiation are the TFs encoded by the *Pax6* and *Sox9* genes. Pax6 is required for the development of most ocular cell types, and haploinsufficiency for Pax6 is the cause of a pan ocular syndrome termed aniridia, which is characterized by iris absence, foveal hypoplasia, nystagmus, cataracts and corneal vascularization leading to keratopathy (Hingorani et al., 2012; Lee and Colby, 2013; Mirzayans et al., 1995; Ton et al., 1991). Pax6 regulates *Mitf* (Bäumer et al., 2003; Bharti et al., 2012) and plays a role, together with Mitf, in pigmentation of the RPE in the early stages of differentiation (Raviv et al., 2014). Sox9 regulates genes of the visual cycle, which are expressed at postnatal stages in the terminally differentiated RPE cells (Masuda et al., 2014). During retinogenesis, Sox9 is expressed in multipotent progenitor cells,

[1]Department of Human Molecular Genetics and Biochemistry, Sackler Faculty of Medicine, Sagol School of Neurosciences, Tel Aviv University, Tel Aviv 69978, Israel. [2]Department of Particle Physics, Raymond and Beverly Sackler School of Physics and Astronomy, Tel-Aviv University, Tel Aviv 69978, Israel. [3]Department of Neurobiology, Biochemistry and Biophysics school, George S. Wise Faculty of Life Sciences, Tel-Aviv University, Tel Aviv 69978, Israel. [4]The Hadassah Human Embryonic Stem Cell Research Center, The Goldyne Savad Institute of Gene Therapy and The Department of Obstetrics and Gynecology, Hadassah-Hebrew University Medical Center, 9112001 Jerusalem, Israel. [5]Department of Molecular Cell Biology, Weizmann Institute of Science 76100, Rehovot, Israel. [6]Department of Genetics, University of Pennsylvania Perelman School of Medicine, 12-126 Smilow Center for Translational Research, 3400 Civic Center Blvd, Philadelphia, PA 19104-6145, USA. [7]Sagol School for Neuroscience, Tel-Aviv University, Tel Aviv 69978, Israel.

*Authors for correspondence (ruthash@post.tau.ac.il; ranel@tauex.tau.ac.il)

P.B., 0000-0002-4042-214X; R.E., 0000-0003-3440-1286; R.A.-P., 0000-0002-5364-6898

Received 22 January 2018; Accepted 2 July 2018

Development (2018) 145, dev163691. doi:10.1242/dev.163691

although in the adult retina it is expressed only in Müller glia and RPE cells (Poché et al., 2008). Both Müller glia and RPE cells are known to secrete growth factors that support the two retinal vascular layers (Bai et al., 2009; Marneros et al., 2005). Moreover, studies in mesenchymal cells indicate that Sox9 promotes angiogenesis and VEGF secretion (Eshkar-Oren et al., 2009), whereas Pax6 was shown to suppress angiogenesis and VEGF expression in glioma cells (Zhou et al., 2010) and in the cornea (Ambati et al., 2006). The possible involvement of Pax6 and Sox9 in vasculature development in the retina or choroid remains so far unknown.

Here, we describe that Pax6-negative regulation of *Sox9* dictates the timing of RPE development as well as choroid maturation. Our results demonstrate that these two pivotal factors are not only controling the timely differentiation of the RPE, but are also important for normal development of the adjacent choroid vasculature. In addition, we found that genes regulated by Sox9 during RPE differentiation are elevated in a cohort of patients in the early stages of AMD (Newman et al., 2012). Thus, our study reveals part of the molecular mechanism that controls the developmental crosstalk between the RPE and the choroid vasculature. Furthermore, we establish the importance of the interplay between these key TFs during normal RPE and choroid maturation, and implicated their involvement in common retinal pathologies.

RESULTS

Pax6 inhibits *Sox9* expression during RPE differentiation

To evaluate how Pax6 and Sox9 control the stepwise differentiation of the RPE, we first analyzed their expression during mouse embryogenesis by immunofluorescence. The expression of the two TFs reflected the progress of the differentiation process. In the early optic cup, Pax6 was detected throughout the RPE (Raviv et al., 2014), but was then gradually replaced by Sox9, which initially appeared near the optic nerve head and eventually reached the optic cup periphery (Fig. 1A, Fig. S1). These expression patterns suggest a possible negative regulatory interaction between *Pax6* and *Sox9*. Indeed, quantitative PCR (qPCR) detected a significant increase of *Sox9* transcripts in RNA isolated from the RPE and adjacent mesenchyme of *Pax6* conditional mutant mice at embryonic day (E) 15.5 (*Pax6*$^{loxP/loxP}$*;DctCre*, termed *Pax6* cKO) compared with controls [Fig. 1B; fold change (FC)=1.62, P=0.0002] and of Sox9 protein in the peripheral optic cup of Pax6 mutant RPE (Fig. S2).

Sox9 is expressed in both the RPE and adjacent mesenchyme. We next examined whether the increase in *Sox9* transcript levels following Pax6 loss reflects a change in transcription specifically in the RPE. To this end, we quantified *Sox9* transcript levels by single-molecule *in situ* hybridization (smFISH) (Lyubimova et al., 2013) in control and *Pax6* cKO RPE at E13.5 (Fig. 1C-E). The transcript levels of *Pax6* and *Sox9* in the controls confirmed the presence of a spatial dose-dependent inverse relationship between *Pax6* and *Sox9*, with a significant negative correlation between the mRNA levels (E13.5, Fig. 1D; Spearman correlation of −0.76, P=0.017). In addition, *Sox9* levels were significantly elevated in *Pax6* cKO RPE (Fig. 1E; average FC=1.41 in RPE cells, P=0.036), supporting the observation of a significant upregulation of *Sox9* transcripts in the absence of Pax6.

Interestingly, despite the overall elevation, the central to peripheral gradient of *Sox9* transcripts was maintained in *Pax6* cKO RPE (Fig. 1E), indicating that although the expression of *Sox9* is inhibited by Pax6, there must be additional factors that contribute to the characteristic central to peripheral gradient of expression. To further substantiate the inhibition of *Sox9* by Pax6, we induced ectopic expression of Pax6 in the RPE by *in vivo* electroporation of an expression vector at postnatal day 0 (P0), at which time Pax6 is not detected in the RPE. This ectopic expression of Pax6 resulted in a downregulation of *Sox9* expression at P4, compared with control cells electroporated with a GFP expression vector (Fig. 1F,G, Fig. S3; FC=0.24, P=0.0001, n=4), thus substantiating the negative regulation of *Sox9* by Pax6.

To further examine whether Sox9 reciprocally regulates *Pax6*, we used the *DctCre* line to inactivate the *Sox9* gene. The expression of *Pax6* in the RPE was analyzed by immunofluorescence (Fig. S4) as well as qPCR in *Sox9*$^{loxP/loxP}$*;DctCre* mice (termed *Sox9* cKO) and controls (*Sox9*$^{loxP/loxP}$). There were no differences in Pax6 levels detected at E13.5 or E15.5 (Fig. 2A,B; FC=1.22, P=0.23). This led us to conclude that Pax6 controls *Sox9* expression and the temporal progression of RPE differentiation, but Sox9 does not inhibit Pax6 expression during RPE maturation.

The Pax6 and Sox9 regulatory relationship controls the timing of RPE maturation

To determine the global contribution of *Sox9* to RPE maturation, we performed RNA sequencing (RNA-seq) analyses of RPE and choroid tissues of *Sox9* cKO and control mice. A comparison of the transcriptomic data from tissues of control mice at E15.5 and P5 revealed robust changes in expression during RPE maturation: more than 2500 differentially expressed genes were detected, with 1093 upregulated and 1635 downregulated at P5 compared with E15.5 (Fig. 2C, Table S1; see Materials and Methods for cutoff criteria). The pronounced transcriptomic differences between E15.5 and P5 reflect differences in the function and activity acquired by the cells during their transition from pigmented epithelial cell precursors to terminally differentiated RPE cells. Gene Ontology (GO) enrichment analysis showed, as expected, that the programs altered at P5 compared with E15 involve visual perception and transporter activity, while there is a decrease in functional categories related to proliferation (Table S2; based on *DAVID*, Huang et al., 2009).

We then compared the transcriptomes of control and *Sox9* cKO mice. At E15.5, the *Sox9* mutant RPE/mesenchyme showed significant [false discovery rate (FDR)<10% and completely separated expression levels between the two genotypes; see Materials and Methods] differential expression of 37 genes, with 31 genes downregulated and six upregulated compared with the control (Table S3). In contrast, at P5, we detected 55 differentially expressed genes (11 downregulated and 44 upregulated in the *Sox9* cKO, Table S4). Next, we examined whether there was any modulation during normal RPE maturation of the genes downregulated at E15.5 in the *Sox9* cKO. Notably, we found that as a set, these genes are significantly activated at P5 compared with E15.5 in control tissue, indicating that they are relevant for the late differentiation stages of the RPE (Fig. 2D, P=1.11E-8). Thus, Sox9 is important for activating genes that are expressed in the late stages of RPE differentiation.

We also examined RPE gene expression profiles in E15.5 *Pax6* cKO and control mice (Raviv et al., 2014). In these mice, 31 genes were elevated and 162 were reduced in mutant compared with control RPE (FDR=5%, see Materials and Methods). GO enrichment analysis showed that the genes downregulated in the *Pax6* cKO mice were mostly associated with melanin biogenesis, which requires Pax6-mediated regulation of *Mitf* activity during early stages of RPE differentiation (Raviv et al., 2014). We found that, as a set, the expression of the genes upregulated in *Pax6* cKO at

Development (2018) 145, dev163691. doi:10.1242/dev.163691

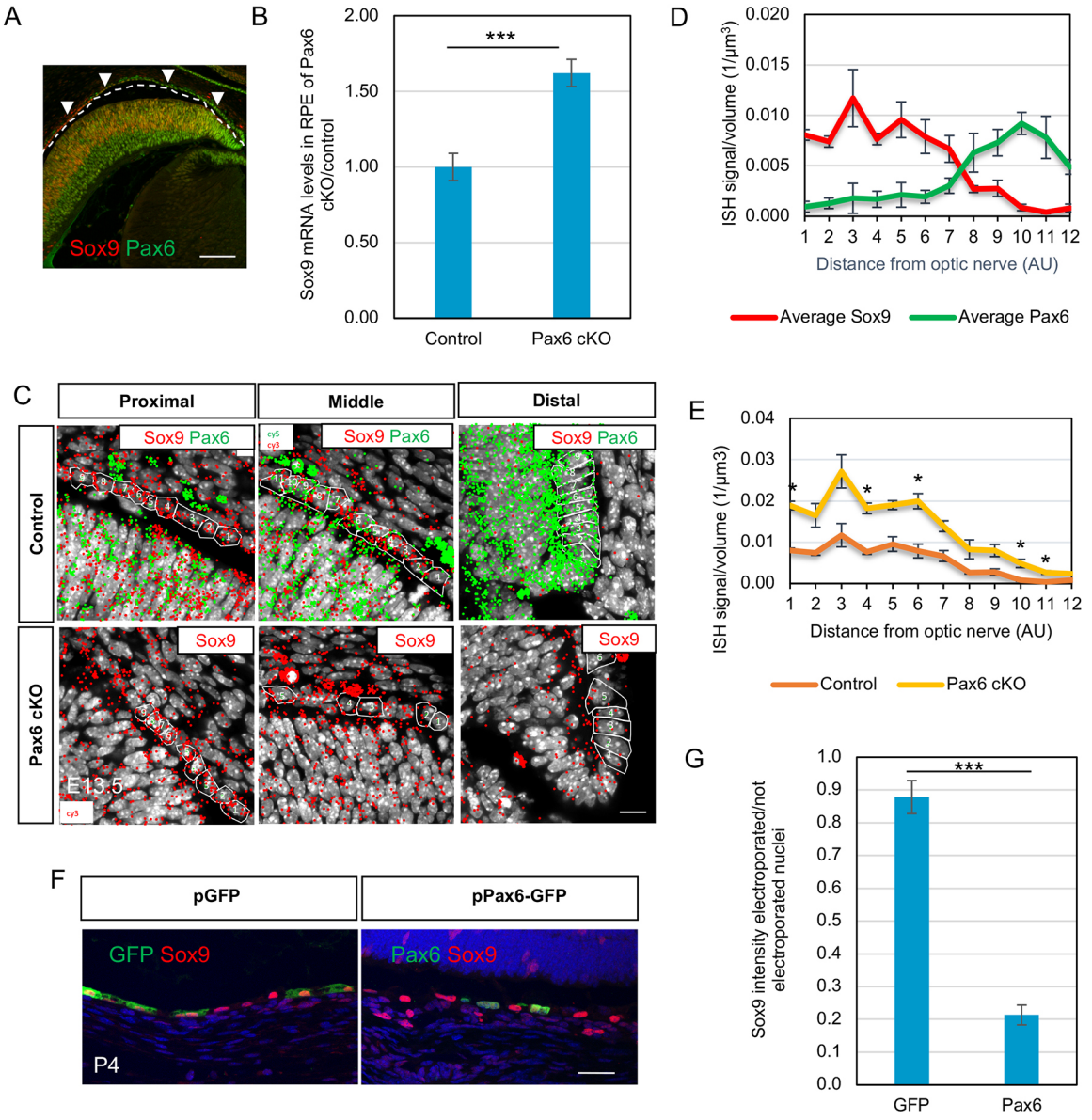

Fig. 1. Pax6 negatively regulates *Sox9* expression in RPE cells. (A) E15.5 control eyes labeled with antibodies against Pax6 and Sox9. The border between the RPE and retina is marked with a dashed line, and arrowheads indicate the RPE layer examined. Scale bar: 100 µm. (B) Relative transcript levels of *Sox9* in RPE of control and *Pax6* cKO E15.5 mice using qPCR (n=4). (C) Example of images from smFISH analyses of *Pax6* and *Sox9* mRNA at E13.5 in control (top), and of *Sox9* transcripts in *Pax6* cKO (bottom) RPE cells. Small white numbers mark the cells that were analyzed in each area. Scale bar: 10 µm. (D) *Pax6* and *Sox9* spatial dosage inhibitory relationship throughout the optic cup. The Spearman coefficient demonstrates a negative correlation between the expression of *Pax6* and *Sox9* (R=−0.76, P=0.01, n=3). (E) Quantitative analysis of *Sox9* expression by smFISH in control and *Pax6* cKO RPE (n=3). (F) Representative images of sections of P4 eyes, which were electroporated at P0 with pCAG-GFP vector (left) or pCAG-GFP together with pCAG-Pax6 (right). The sections were stained for GFP, Sox9, Pax6 and 4′,6-diamidino-2-phenylindole (DAPI). Scale bar: 25 µm (separate channels in Fig. S3). (G) Quantification of the ratio of Sox9 average fluorescence intensity in electroporated nuclei compared with unelectroporated nuclei (n=4). Data are mean±s.e.m.; *P<0.05, ***P<0.005.

E15.5 was induced during normal RPE maturation between E15.5 and P5 (Fig. 2E, P=4.46E-09, Table S5), indicating that these genes too are involved in the late differentiation stages of the RPE. This supports the proposal of a suppressive effect of Pax6 on the expression of RPE maturation genes at E15.5, in line with the suppression of *Sox9* by Pax6 (Fig. 1). Finally, the genes downregulated relative to control in *Sox9* cKO at E15.5 (RPE maturation genes) were, as a set, de-repressed in *Pax6* cKO relative to control (Fig. 2F, P=4.11E-4), thus supporting the notion that Pax6 controls the temporal differentiation of the RPE, at least partly, by inhibition of *Sox9*.

Pax6 and *Sox9* expression in the RPE is required for choroid development

The RPE is crucial for choroid development via polar secretion of VEGF (Blaauwgeers et al., 1999). Corresponding with the co-development of RPE and choroid vasculature, we found that, as a set, the expression of genes involved in angiogenesis (as defined by GO, Huang et al., 2009) was significantly elevated between E15.5 to P5 in the RPE/mesenchyme of control mice [Fig. 2G, Table S6; e.g. *Vegfa* increased 2.16-fold, P=2.42E-12; angiopoietin-like 4 (*Angptl4*) increased 2.11-fold, P=6.7E-4]. As the transcriptomic changes we observed in mouse tissue could also represent

Development (2018) 145, dev163691. doi:10.1242/dev.163691

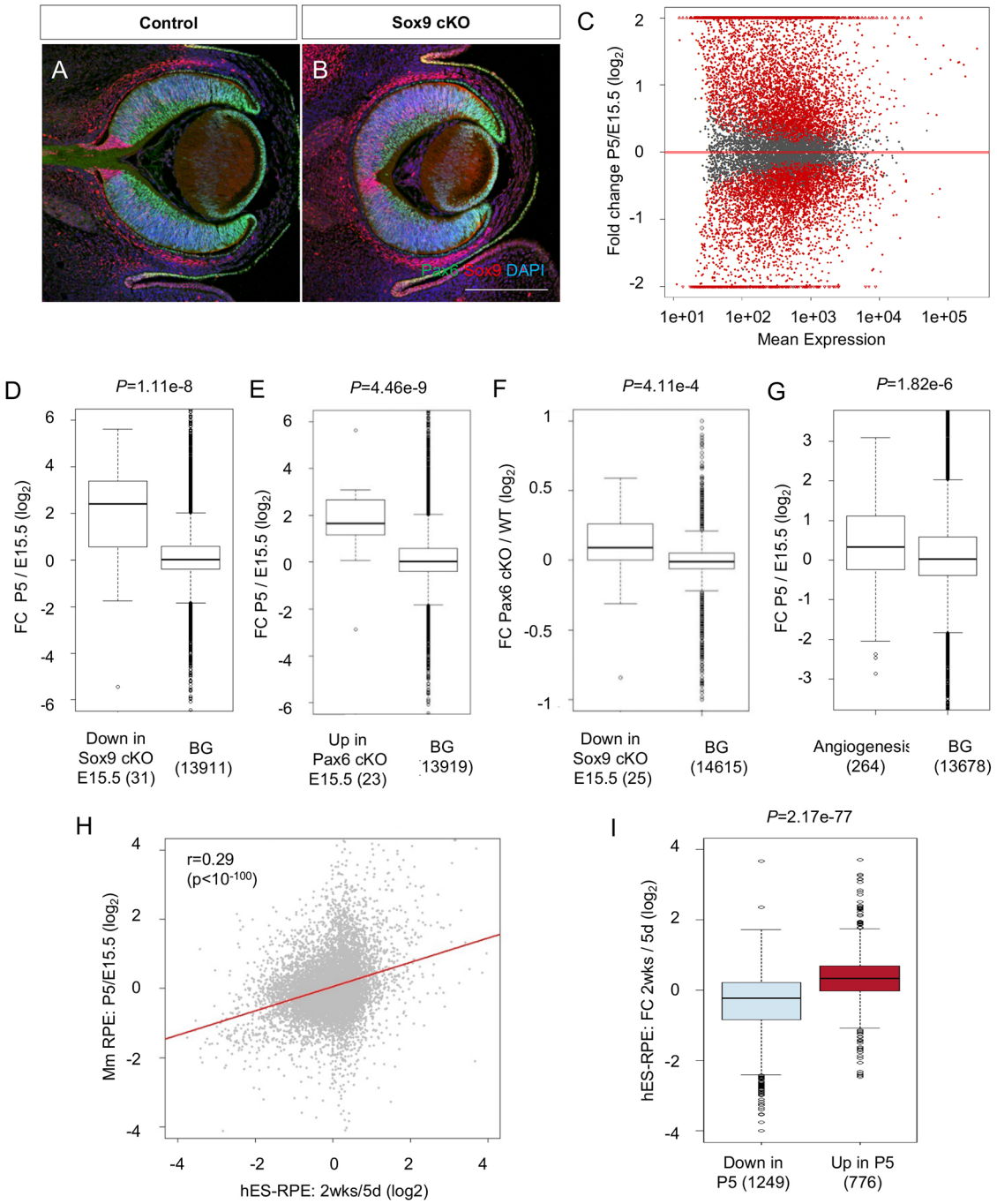

Fig. 2. Sox9 activates and Pax6 inhibits the expression of late RPE genes. (A,B) Immunofluorescence analyses of Pax6 and Sox9 in RPE in E13.5 (A) control and (B) *Sox9* cKO mice. Scale bar: 250 µm. (C) MvA plot comparing gene expression of control RPE/mesenchyme cells measured at E15.5 and P5. Genes demonstrating a significant change in expression (FDR<0.05) are shown in red. (D-G) The distributions of fold change (FC) between a specified target set and a background (BG) set of genes using Wilcoxon's test. (D) FC distribution in P5 vs E15.5 controls is compared between genes that were downregulated in E15.5 *Sox9* cKO (the target set) and all remaining genes in the dataset (BG set). (E) FC distribution in P5 vs E15.5 controls is compared with the genes that were upregulated in E15.5 *Pax6* cKO (the target set) and all other genes in the dataset (of 31 genes that were detected as upregulated in *Pax6* cKO microarray, 23 genes with robust detection in the RNA-seq data measured in the current study were included in this analysis). (F) FC distribution in E15.5 *Pax6* cKO versus control littermates is compared between the set of 25 genes that were downregulated in *Sox9* cKO and detected by the microarray data (the target set) and all other genes in the dataset. (G) FC distribution in P5 vs E15.5 controls is compared between a target set consisting of genes assigned to the 'angiogenesis' GO functional category (the target set) and all the other genes in the dataset. (H) Significant Spearman correlation between changes in the transcriptome measured in developing mouse RPE and during hES-RPE differentiation of d5 compared with d14. This analysis includes 10,244 genes that were detected in both the mouse RPE (RNA-seq) and human hES-RPE (expression arrays) datasets; human genes were mapped to their mouse homologs using ENSEMBL Hs-Mm homology map. (I) The sets of genes that were significantly up- and downregulated during mouse RPE development showed significant induction and repression during differentiation of the hES-RPE system (Wilcoxon's test). For all boxplots, the bottom and top of the box indicate the lower and upper quartiles, respectively. The bar within the box indicates the median. The upper and lower whiskers are 1.5 interquartile-range (IQR) above and below the top and bottom of the box. Outliers beyond the whisker limits are presented by dots.

Development (2018) 145, dev163691. doi:10.1242/dev.163691

differences in the composition of the mesenchyme in the vicinity of the samples obtained at different differentiation stages, we further analyzed the transcriptome of RPE generated from human embryonic stem cells (hES-RPE cells) (Idelson et al., 2009). The stem cell-derived human RPE mimics differentiated RPE and these are currently being tested in clinical trials (Amram et al., 2017; Song and Bharti, 2016). The hES-RPE cells partially dedifferentiate following splitting and thus provide a good model to study the mechanisms of differentiation in culture (Liao et al., 2010). We analyzed the transcriptomic changes between cells from 5 days (d5) after splitting, a stage at which the cells are partially dedifferentiated (evidenced by reduced pigmentation and the absence of hexagonal morphology), and differentiated cells after 14 days (d14) in culture (Table S7). Our results revealed a significant correlation between the changes observed during RPE differentiation in mice and hES-RPE (Fig. 2H,I). Corresponding to the findings in mice, we observed that *Sox9* levels were elevated (4.1-fold, P=1.8E-5) during the *in vitro* differentiation of hES-RPE cells, whereas *Pax6* levels were reduced (0.7-fold, P=0.016). Moreover, the levels of the angiogenesis factors *Vegfa*, *Vegfb* and *Angptl4* were increased (2.7-, 2.5- and 4.4-fold, respectively, P<0.01) corresponding with their expression in the developing mouse RPE/choroid.

Association between either *Pax6* or *Sox9* and angiogenesis was demonstrated in other tissues, including the cornea (Ambati et al., 2006), glioma (Zhou et al., 2010) and skeleton mesenchymal cells (Eshkar-Oren et al., 2009). To investigate the possible involvement of these early and late RPE TFs in choroid vasculature development, endothelial cells (ECs) were labeled with isolectin B4 (IsoB4), and the vascular area was quantified at E15.5. This analysis demonstrated an early reduction in the IsoB4-labeled area in the *Pax6* cKO mice compared with controls (Fig. 3A-C, FC=0.61, P=0.027), but there were no significant changes detected in the IsoB4 labeling in the *Sox9* cKO mice (Fig. 3C, P=0.085), which is in agreement with its late roles in RPE differentiation.

Nevertheless, our transcriptomic analysis at P5 did reveal a very significant downregulation of angiogenesis genes in RPE from *Sox9* cKO mice compared with controls (Fig. 3D), indicating a role for Sox9 in the regulation of angiogenic factors during the late stages of RPE development. Indeed, the distribution of vascular endothelial cadherin (VE-Cad; Cdh5 – Mouse Genome Informatics) was reduced in the *Pax6* cKO mutants, and elevated in the *Sox9* cKO mutants at P5 (Fig. 3E-I), supporting the involvement of both factors in the regulation of the amount of choroidal endothelium as well as its adhesion properties.

Our next objective was to determine the architecture of the choroid vascular network in detail, and to quantify the density of the choroid vasculature in control and *Pax6* and *Sox9* mutant mice. To this end, we performed cardiac perfusions with fluorescein isothiocyanate (FITC)-conjugated albumin in order to fill and fix the vasculature with fluorescent gel. This was followed by optical sectioning of the sample, reminiscent of the technologies used to image vasculature in the brain (Tsai et al., 2009). In the control mice, the CC was a thin mesh network (Fig. 4A-C) as observed in previous studies (Fryczkowski, 1994; Saint-Geniez and D'Amore, 2004). The long and short posterior ciliary arteries, as well as the vortex veins, were observed in both *Pax6* cKO and *Sox9* cKO mice (Fig. 4A-I,J), demonstrating that the initial vascular network develops normally in both mutants.

To examine the effect of the RPE mutations on choroid development more closely, it was necessary to perform

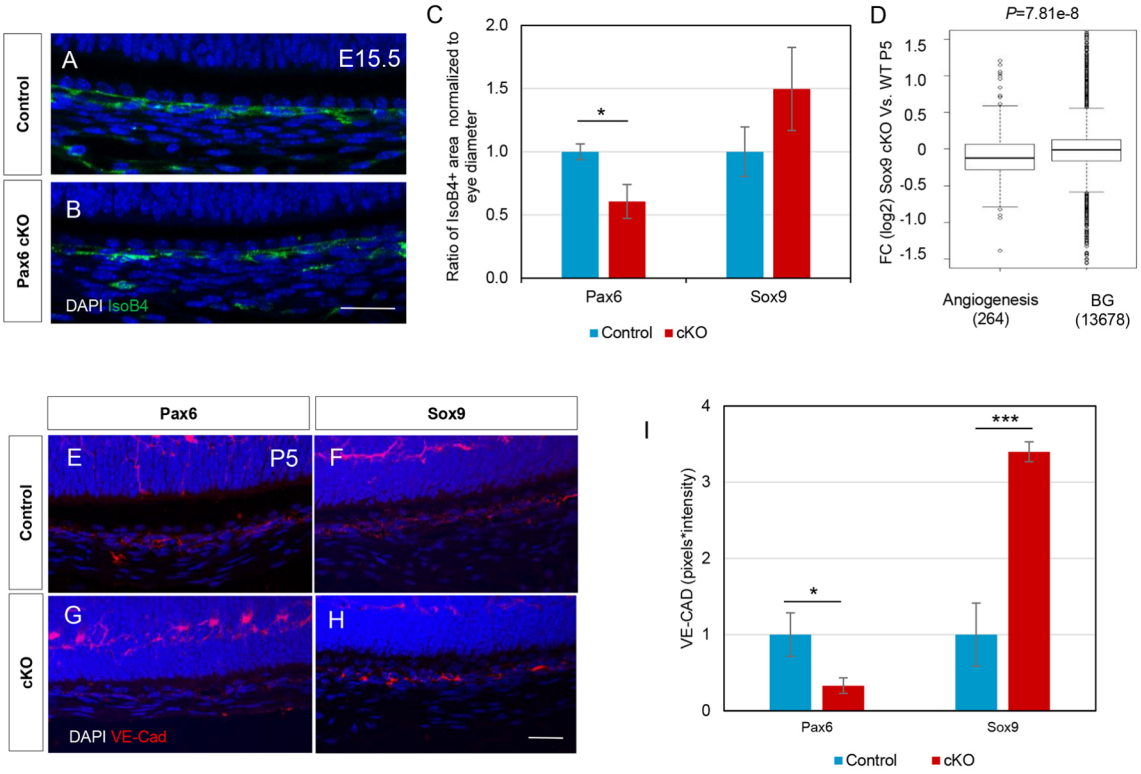

Fig. 3. *Pax6* and *Sox9* expression in the RPE is required for choroid development. (A-C) Antibody labeling for IsoB4$^+$ choroid vascular layers of (A) control and (B) *Pax6* cKO (E15.5) mice was quantified (C) using ImageJ and normalized to eye diameter (n=8 per group). Scale bar: 25 µm. (D) Analysis of the transcriptional changes of angiogenesis markers in P5 *Sox9* cKO RPE and choroid. (E-H) Control (E,F), *Pax6* cKO (G), and *Sox9* cKO (H) mice at P5 labeled with antibodies against VE-Cad. Scale bar: 25 µm. (I) Quantification of VE-Cad staining using ImageJ (n=3). Data are mean±s.e.m.; *P<0.05, ***P<0.005.

Development (2018) 145, dev163691. doi:10.1242/dev.163691

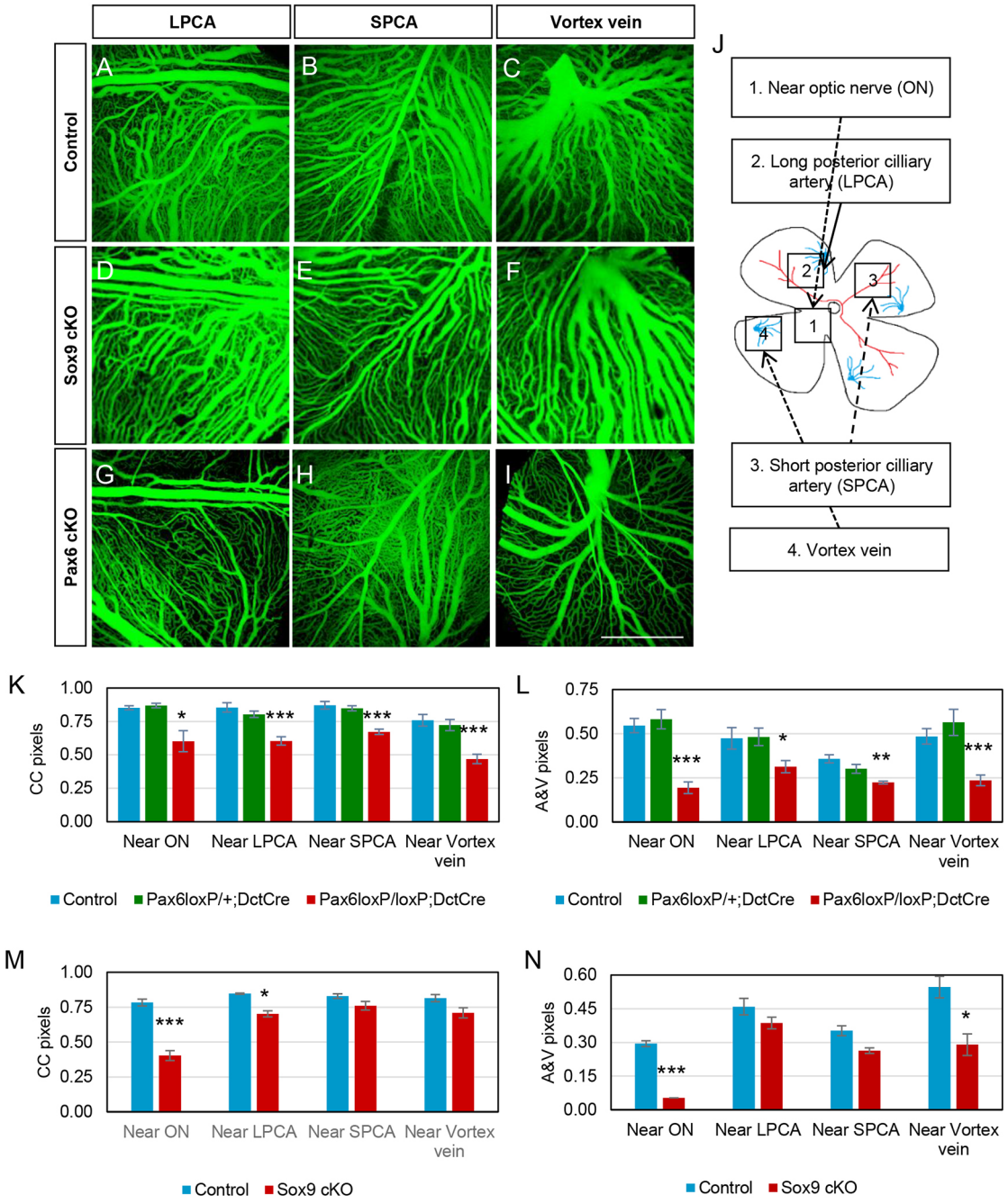

Fig. 4. Quantification of choroid vascular layers using CapMan, a BDT machine learning algorithm tool. (A-I) Choroid vasculature of P21 control (A-C), *Sox9* cKO (D-F) and *Pax6* cKO (G-I) mice evaluated after cardiac perfusion of FITC-labeled albumin; eyes were dissected, flat-mounted, and imaged using confocal microscopy. Scale bar: 250 µm. (J) A scheme illustrating imaged areas of the choroid. (K,L) Quantification of pixels in the vascular areas of the CC layer (K) and A&V (L) of the choroid in *Pax6* mutants compared with controls (n=5). (M,N) Quantification of differences in the vascular area of the CC layer (M) and A&V (N) of the choroid in *Sox9* mutants compared with controls (n=5). Data are mean±s.e.m.; *P<0.05, **P<0.01, ***P<0.005.

quantitative analyses of the different choroidal layers. To address the challenge of assigning pixels to individual vascular layers, we developed an automated tool called CapMan that employs a machine learning algorithm to segregate signals deriving from the arteries and veins (A&V) from those deriving from the CC (Fig. 4, Materials and Methods). The threshold between the two layers was automatically optimized by training the algorithm on sample images according to pixel intensity, as well as including features designed to measure vessel length and diameter. The use of a combination of these features resulted in a higher accuracy than considering each one separately (Fig. S5). The results from CapMan are presented as the ratios of A&V pixels to all pixels in the image, and CC pixels to all pixels minus the A&V pixels. Ratios were used rather than the absolute vascular area in each layer in order to avoid biases that result from masking between the layers. This pixel-wise approach exposes alterations in the delicate layer of the capillaries that are otherwise masked by the arteries and veins, and could also be useful for evaluating the vascular phenotypes in other mutants.

Using CapMan, we quantified the changes in different areas observed in the choroid of *Pax6* and *Sox9* mutants (Fig. 4J). First,

Development (2018) 145, dev163691. doi:10.1242/dev.163691

we compared both *Pax6* cKO and *Pax6*$^{loxP/+}$*;DctCre* mice with their control littermates. The examination of the heterozygous mutants was important because only one *Pax6* allele is mutated in patients with aniridia. The results of our analysis showed that both the CC and A&V of the cKO heterozygous mice were normal (Fig. 4K,L). In contrast, all four of the anatomical regions analyzed in the homozygous *Pax6* cKO mice had reduced vascularity in both CC (average FC=0.7, *P*=0.001) and in the A&V (average FC=0.53, *P*=0.02) (Fig. 4K,L). A similar analysis conducted in the *Sox9* cKO mice revealed significant changes in both vascular layers near the optic nerve head, as well as a reduction in the vascular area in the other three regions imaged (Fig. 4M,N). This difference reached significance in the CC near the long posterior ciliary artery (average FC=0.78, *P*=0.048) as well as in the A&V near the vortex vein (average FC=0.58, *P*=0.043).

Sox9 and Pax6 targets in the RPE regulate choroid differentiation and are associated with AMD

The reduction in vascular area in both the *Pax6* and *Sox9* RPE mutants indicates that these TFs play a role in the regulation of genes and processes important for normal development of the adjacent choroid. Because changes in the RPE and vasculature are characteristic of AMD (Bhutto and Lutty, 2012), it was of interest to examine whether the role proposed for RPE TFs in choroid differentiation could contribute to the understanding of AMD pathogenesis. Newman et al. conducted gene expression profiling on human RPE-choroid tissues derived from different stages of AMD (pre-, dry and wet AMD) and geographic atrophy, as well as from healthy individuals, and defined gene clusters that were up- or downregulated in each stage (Newman et al., 2012). We focused our analysis on genes regulated by Sox9, which is active during the late stages of differentiation and in the adult RPE. Hence, we compared the transcriptomic changes in *Sox9* cKO mice (P5) to the alterations observed in AMD patients (Newman et al., 2012). Examination of the expression of the mouse orthologs of these gene clusters in our *Sox9* cKO RNA-seq data revealed that the genes upregulated in the pre-AMD phase were significantly downregulated in *Sox9* cKO at P5 (*P*=1.16E-6, Fig. 5A, Table S8), suggesting, but not yet proving, involvement of these genes in AMD pathology.

To further inspect which of the genes that are upregulated in pre-AMD could be directly regulated by Sox9, we intersected this gene set with the set of Sox9 target genes derived from Sox9 chromatin immunoprecipitation sequencing (ChIP-seq). (ChIP-seq) analysis in differentiated (d14) hES-RPE. The ChIP-seq analysis revealed 1146 Sox9 peaks, which were mapped to 941 genes (based on nearest promoter, Table S9). The location distribution of Sox9 binding sites showed marked peak near genes transcription start sites (TSS, Fig. 5B). In addition, *de novo* motif analysis identified a CCAAT motif as highly enriched in the promoters bound by Sox9. This motif was also identified as the top scoring motif by a previous study that profiled Sox9 binding sites in a colorectal cancer cell line (Fig. 5C) (Shi et al., 2015). This motif diverged from the *in vitro* bound site (Mertin et al., 1999), which is in agreement with the previous ChIP-seq studies that documented different motifs for Sox9 (Bhandari et al., 2012; Kadaja et al., 2014; Oh et al., 2010). The observed divergence from the *in vitro* motif probably reflects the context specific activity, which is dependent on different interacting partners of the Sox proteins (reviewed in Kamachi and Kondoh, 2013).

Intersection between Sox9 ChIP-seq peaks and genes upregulated in pre-AMD pointed to eight genes from the pre-AMD set as targets of Sox9. Notably, the expression of seven of these eight genes was attenuated in *Sox9* cKO compared with control RPE at P5 (Fig. S6, Table S10). Although the reduction for most of these seven genes was modest and did not reach statistical significance, as a set, this decreased expression is significant (7/8; *P*=0.035, binomial test).

One of the genes identified in this pre-AMD gene cluster (Table S8) and indicated by the ChIP-seq analysis as a direct target gene of SOX9 (Table S9) is *ANGPTL4*. *ANGPTL4* is a member of the angiopoietin family of secreted proteins, known to be involved in the regulation of metabolism and angiogenesis (Tan et al., 2012). Validation of SOX9 binding to the promoter of *ANGPTL4* was performed by ChIP-PCR in hES-RPE, as well as examination of possible association to this region by PAX6. Significant binding of both TFs was detected on the first exon of *ANGPTL4* (Fig. 5D,E; PAX6 fold enrichment 8.95, *P*=0.025, and SOX9 fold enrichment 8.52, *P*=0.008).

Angptl4 was recently reported to promote vessel maturation and permeability, at least partly by modulating vascular junction properties, and to be involved in diabetic eye diseases (Babapoor-Farrokhran et al., 2015; Huang et al., 2011; Sodhi et al., 2015). Our RNA-seq data showed that the expression of *Angptl4* increased between E15.5 and P5 in control mice (FC=2.12, *P*=6.7E-4, Table S1), as well as during differentiation of hES-RPE cells (FC=4.4 from d5 to d14, Table S7), thus suggesting *Angptl4* involvement in late stages of RPE maturation. Quantification of the levels of the *Angptl4* transcript by qPCR confirmed that the expression of *Angptl4* was significantly reduced in *Sox9* cKO mice at P5 (FC=0.64, *P*=0.001). In contrast, there was a significant increase in expression in *Pax6* cKO mice (FC=1.54, *P*=0.035) compared with control mice at E15.5 (Fig. 5F). This suggests that *Angptl4* is oppositely regulated by these two TFs (Fig. 6).

In conclusion, our findings reveal that Pax6 reduction in the RPE is important for timely elevation of Sox9, which is a key transcription factor for RPE maturation. Moreover, both Pax6 and Sox9 are important for choroid vasculature differentiation and their downstream targets, including Angptl4, should be considered as candidates involved in choroid and retinal pathologies in adults.

DISCUSSION

This study describes the temporal expression of RPE TFs and their role in the synchronized maturation of the RPE and neighboring blood vessels. Here, we find that *Pax6* controls the timing of both RPE and choroid coordinated differentiation, partly through negative regulation of *Sox9* (Fig. 6). Inhibition of various targets by Pax6 has been shown to be required for acquisition and maintenance of cell fate in different lineages: in developing and adult beta-cells, Pax6 seems to directly inhibit the expression of competing endocrine lineages (Ahmad et al., 2015; Hart et al., 2013; Swisa et al., 2016); in the retina, Pax6 is thought to prevent the premature expression of the neural precursor genes *Mash1* (*Ascl1*) and *Crx* in retinal progenitor cells (Klimova and Kozmik, 2014; Oron-Karni et al., 2008; Philips et al., 2005); while in the lens, part of Pax6 inhibition of gene expression is mediated by activation of *miR-204* (Shaham et al., 2013).

Sox9 is known to regulate the expression of visual cycle genes and to be involved in the late stages of RPE differentiation (Masuda et al., 2014). The overlap in gene expression revealed by our analysis of the transcriptomes of the RPE and choroid of *Sox9* cKO mice at E15.5 and P5 could reflect the different programs expressed in RPE precursor cells and terminally differentiated cells. Comparisons with control transcriptomes identified additional

Development (2018) 145, dev163691. doi:10.1242/dev.163691

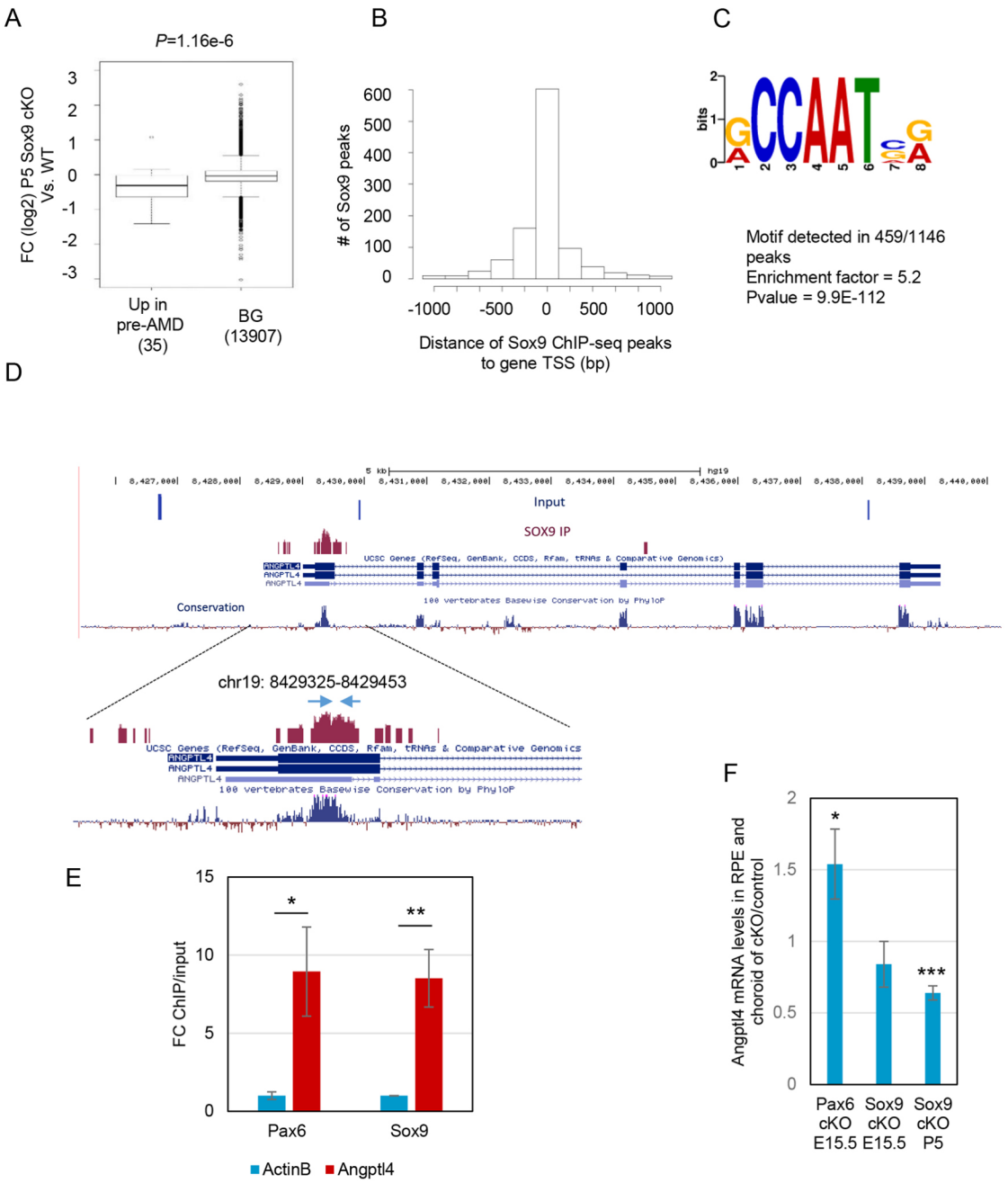

Fig. 5. Sox9 targets are upregulated in pre-AMD and are candidates for mediating choroid vascular development. (A) The cluster of genes that were upregulated in pre-AMD patients (Newman et al., 2012) is significantly downregulated in the *Sox9* cKO mouse model at P5. The human genes in the 'up in pre-AMD' cluster were mapped to their mouse orthologs, and then FC distribution in *Sox9* cKO versus control at P5 was compared between the 'up in pre-AMD' cluster (the target set) and all the rest of genes in the dataset (BG set) using Wilcoxon's test. Of the 58 human genes that were detected as upregulated in pre-AMD, the expression of 35 was robustly detected in our RNA-seq *Sox9* cKO data, and these are included in this analysis. (B) ChIP-seq analysis of SOX9 binding sites in hES-RPE at d14. The histogram of the location of SOX9 binding sites shows a marked peak towards genes' TSS with preferential binding within 100 bp of the TSS. (C) The top sequence motif identified in the genomic regions bound by Sox9 in hES-RPE. (D) The locations of the ChIP primers and the evolutionary conservation in this region of the *Angptl4* promoter identified to be bound by Sox9 by ChIP-seq [PhyloP method on 100 vertebrates (Cooper et al., 2005)]. (E) ChIP-PCR with SOX9 antibodies against SOX9 and PAX6 in d14 hES-RPE, comparing to enrichment by ActinB (ACTB) (E, *n*=3). (F) Levels of *Angptl4* in the RPE of E15.5 *Pax6* cKO, E15.5 and P5 *Sox9* cKO relative to levels in control RPE/mesenchyme (*n*=4). Data are mean±s.e.m.; **P*<0.05, ***P*<0.01, ****P*<0.005.

genes that might be regulated by Sox9 to promote RPE maturation. These include *Slc16a8*, which encodes the monocarboxylate transporter, *Rrh*, encoding the RPE peropsin, which functions in retinoid processing (Cook et al., 2013), and *Cst3*, which has been linked to AMD and choroidal neovascularization (Zurdel et al., 2002a,b).

Cooperation between Pax6 and another member of the Sox family, Sox2, has been described previously (Kondoh and Kamachi, 2010). Sox2 and Pax6 were shown to trigger the early lens differentiation program (Kamachi et al., 2001), and to cooperate in regulating genes required for proper optic cup morphogenesis at the later stage of optic pit formation (Smith et al., 2009). Inhibitory

Development (2018) 145, dev163691. doi:10.1242/dev.163691

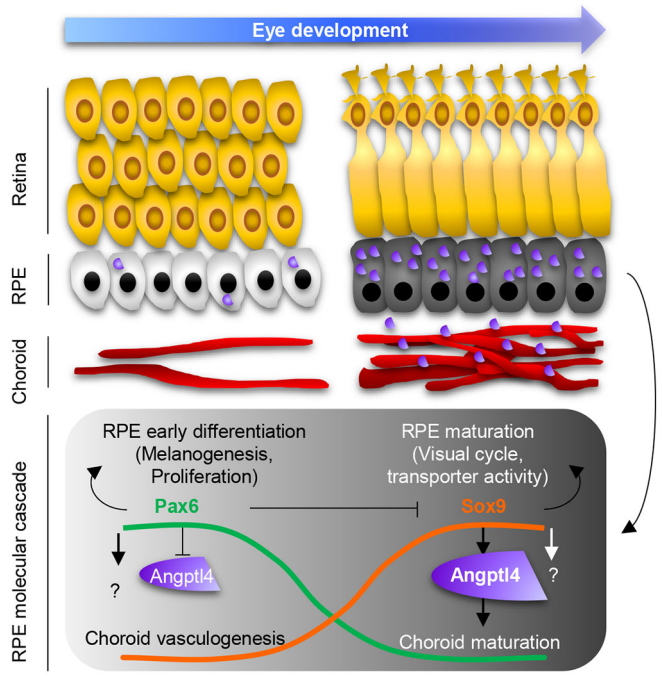

Fig. 6. The RPE TFs, Pax6 and Sox9, control early and late events in RPE and choroid vasculature development. RPE differentiation is temporally regulated, with Pax6 required for early stages of differentiation (melanogenesis), whereas Sox9 regulates late differentiation programs (visual cycle genes, transporters, angiogenic factors). Pax6 inhibition of *Sox9* is required for timely expression of late differentiation genes, including factors that affect choroid vasculature differentiation as exemplified by the regulation of *Angptl4*.

regulation of *Sox2* by Pax6 was reported during later stages of lens differentiation (Shaham et al., 2009), and in retinal progenitor cells, the *Sox2* heterozygous mutation results in upregulation of Pax6 (Matsushima et al., 2011). Here, we showed that Pax6 negatively regulates *Sox9* in the RPE to promote early aspects of differentiation, while preventing the premature onset of late differentiation programs.

Further support for the importance of Pax6 in regulation of RPE maturation through inhibition of *Sox9* comes from our finding that genes downregulated in *Sox9* cKO mice at E15.5 were observed to be upregulated in *Pax6* cKO mice at the same stage (Fig. 2F). Amongst these genes are *Rdh10* (*Pax6* cKO FC=1.29 relative to control, *P*=0.031; *Sox9* cKO FC=0.41, *P*=9.34e-19), and *Ttr* (*Pax6* cKO FC=4.32, *P*=0.0001; *Sox9* cKO FC=0.06, *P*=9.55e-184). Both *Rdh10* and *Ttr* genes encode proteins required for retinol processing, supporting our hypothesis that the negative regulatory circuit between Pax6 and Sox9 plays a role in RPE maturation. In the brain, Ttr is synthesized by the choroid plexus epithelium (Herbert et al., 1986), whereas in the eye, *Ttr* mRNA is exclusively expressed by the RPE (Dwork et al., 1990). From the RPE, Ttr is secreted to other ocular structures such as the choroid, and is considered a marker for CC differentiation (Songstad et al., 2015). Mutations in *Ttr* lead to ocular amyloidosis in the familial amyloidotic polyneuropathies (Andrade, 1952), and the mutated protein inhibits the production of angiogenesis factors in the choroid (Nunes et al., 2013).

It is important to note that our results indicate that there are other factors in addition to Pax6 involved in the regulation of *Sox9* expression and eventual RPE differentiation. First, the smFISH data revealed that the spatial expression gradient of *Sox9* was maintained throughout the RPE even in *Pax6* cKO mice. Second, only some of the Sox9 regulated genes were upregulated in the *Pax6* mutant RPE. Factors such as the Wnts and BMPs (Carpenter et al., 2015; Hägglund et al., 2013), as well as Otx2 and Mitf (Masuda and Esumi, 2010), have been implicated in regulating RPE differentiation, and to interact with Pax6 or Sox9. Thus, these factors could also contribute to temporal regulation of RPE differentiation.

Developmental crosstalk between the vascular and nervous systems has already been described in the inner retinal vascular layer (Kurihara, 2016; Okabe et al., 2014). Here, we focused on the guidance of the neuroepithelial RPE cells on the outer vascular layer. Our data demonstrate an upregulation of angiogenesis markers during RPE differentiation, which is in line with previous reports suggesting a role for angiogenesis from mid-gestation, in CC remodeling and their anastomosis with intermediate vessels (Lutty et al., 2010). Four stages of angiogenesis were described: matrix degradation, EC migration, proliferation and vessel morphogenesis via recruitment of pericytes or the creation of fenestrations (Goodwin, 2007). Our findings support this step-wise theory of choroid development because mutation of *Pax6*, which encodes the early RPE TF, disrupted early stages of choroid development and thus resulted in a more severe phenotype of the choroid than *Sox9* mutation.

The results of our analysis of the choroid vasculature of heterozygous *Pax6* cKO mice using CapMan demonstrated that proper vessel development occurred even when one allele of *Pax6* was deleted. Nevertheless, possible choroidal abnormalities in patients with aniridia cannot be ruled out because the *Pax6* mutation in the cKO mice occurs after initial specification of the RPE (Davis et al., 2009). It is therefore possible that haploinsufficiency for *Pax6* affects early events in choroidal development, which were not examined in the current study. Future efforts are needed to determine how Pax6 reduction in RPE progenitors influences the progressive blindness observed in aniridia.

This is one of the first reports that describes the roles of specific TFs in the development of the choroid. Thus far, studies in this field have focused on the importance of RPE secretion of VEGF into the choroid in order to initiate and maintain its development (Marneros et al., 2005; Saint-Geniez et al., 2009; Sakamoto et al., 1995; Zhao and Overbeek, 2001). Several novel candidates for the mediation of choroid development were suggested by this study. One is *Angptl4*, which is an emerging therapeutic target in cancer (Tan et al., 2012) and diabetic retinopathy (Sodhi et al., 2015). We report that *Angptl4* is regulated by both Pax6 and Sox9 in the RPE (Figs 5 and 6), and propose its possible involvement in choroid vascularization. The finding that elevated *Angptl4* expression is associated with early stages of AMD (Newman et al., 2012) further supports the importance of regulating its expression to ensure normal function of the choroid-RPE-retina complex, also in the adult organism.

A recent, parallel study reported that Aldh1a1 from the neuroretina regulates *Sox9* levels in the RPE and, in turn, Sox9 is required for proper choroid differentiation (Goto et al., 2018). Although, according to Goto et al., the phenotype of the Sox9 mutant RPE is restricted to the dorsal choroid, which seems to be more severe than observed by us, this is probably caused by differences in genetic background and/or pattern of Cre activity. Nevertheless, these results provide independent support for our observations on the role of Sox9 in choroid differentiation. The study by Goto et al. suggested, from experiments conducted in

Development (2018) 145, dev163691. doi:10.1242/dev.163691

cultured cells, that Sox9 functions through the regulation of *Vegfa*. We, however, did not detect a reduction in *Vegfa* expression in the *Sox9* cKO mutants based on RNA-seq, nor an association of Sox9 with *Vegfa* regulatory sequences in hES-RPE. In contrast, our findings implicate additional targets of Sox9, such as *Angptl4*, as possible players in choroid differentiation and pathogenesis.

This study revealed a novel developmental mechanism by which regulatory relationship between key TFs in a specific cell lineage regulates the gradual and synchronized differentiation of neighboring tissues. Uncovering the processes leading to choroid differentiation is important for advancing our understanding of normal and pathological processes in eye development, as well as in the retinal-vascular pathologies that appear during aging.

MATERIALS AND METHODS

Mouse lines

The *Sox9*^{loxP} (Akiyama et al., 2002), *Pax6*^{loxP} (Ashery-Padan, 2000) and *DctCre* (Davis et al., 2009) mouse lines have been described previously. In each analysis, loxP/loxP littermates lacking the *DctCre* were used as controls. The genetic background of the mice used in this study was outbred ICR, except for those used in RNA-seq assays, which were kept on a C57BL/6J background to allow dissection of embryonic RPE. Mice were maintained according to international guidelines, and their use was approved by the Tel Aviv University review board.

Immunofluorescence

Immunofluorescence analysis was performed on 10-µm paraffin sections as described previously (Ashery-Padan, 2000), using the following primary antibodies: mouse anti-Pax6 (1:20, Santa Cruz Biotechnology, SC-32766), rabbit anti-Sox9 (1:200, Chemicon, ab5535), rabbit anti-VEGFR2 (1:200, Cell Signaling Technology, 55B11), rabbit anti-VEGF (1:50, Thermo Fisher Scientific, RM-9128), goat anti-Angptl4 (1:100, Santa Cruz Biotechnology, SC-32184), goat anti-VE-cadherin (1:200, Santa Cruz Biotechnology, SC-6458) and rabbit anti-Ki-67 (1:100, Thermo Fisher Scientific, RM-9106). Sections were also labeled with IsoB4 (1:100, Vector Laboratories, FL-1201). Secondary antibodies used were donkey anti-rabbit/goat conjugated to Alexa Fluor 594 (1:1000, Invitrogen, A21207, A11058), and donkey anti-mouse (1:1000, Invitrogen, A21202) conjugated to Alexa Fluor 488.

smFISH

smFISH assays were performed on E13.5 cryosections using DNA probes conjugated to Cy5 for Pax6, or Alexa Fluor 594 for Sox9 (Biosearch Technologies). Imaging was performed using a Leica SP8 confocal microscope. The area between the optic nerve and the optic cup tip in three eyes of control and mutant mice was arbitrarily divided into 12 regions of the same size. The cell borders were determined by phalloidin staining (A12379, Thermo Fisher Scientific). In each of the 12 regions, we quantified all cells that did not overlap with other cells in the *z*-stack acquisition in order to achieve a reliable quantification of the specific transcript level in a single cell. Automatic analysis of the cell borders and transcript levels in each cell were performed using MATLAB (MathWorks) scripts as documented previously (Lyubimova et al., 2013). The average transcript levels were calculated from the values of five to 12 cells in each of the 12 regions.

Differentiation of hES-RPE

For RPE differentiation, hES colonies (Hes1 hES) (Reubinoff et al., 2000) were picked up using collagenase IV (1 mg/ml; 200 U/mg, Gibco-BRL), and cultured as described (Idelson et al., 2009) using a differentiation protocol including treatment with nicotinamide and activinA. After 6-10 weeks in suspension, pigmented clusters were triturated, plated on gelatin (Sigma-Aldrich)-coated plates (Corning Incorporated) and cultured in Knockout medium with 10 mM nicotinamide for 3-5 weeks. The RPE cell lines were further propagated using TrypLE Select (Gibco-BRL). The cells were passaged every 2 weeks.

RNA isolation and reverse transcription

RPE and choroid tissue were isolated as described elsewhere (Raviv et al., 2014) and the E15.5 tissues from control or mutant pups of the same litter were pooled following determination of the genotype. RNA was extracted using QIAshredder and RNeasy kits (Qiagen), and was subjected to reverse transcription using a qScript cDNA synthesis kit (Quanta Biosciences).

Gene expression analysis

Analysis of gene expression in *Pax6* cKO mice was conducted using previously published microarray data (Raviv et al., 2014). Differential expression analysis of the expression array data was performed using SAM (Tusher et al., 2001) as implemented by the samr R package. Global gene expression profiles in hES-RPE at d5 and d14 were measured using Affymetrix GeneChip human GENE 1.0 ST arrays. Three independent biological replicates were performed for each stage in the Microarray Unit of the Cancer Research Center, Sheba Medical Center (Tel Aviv, Israel), according to the manufacturer's procedure (Affymetrix). Gene expression levels were derived using the RMA method implemented in Affymetrix Console. The expression of 13,844 genes was robustly detected (expression of at least 7.0 arbitrary units in at least one sample). Expression levels were further normalized using quantile normalization. To avoid inflation of fold-change estimates for lowly expressed genes, the first quartile (Q1) of the expression distribution was calculated, and all levels below Q1 level were set to this level. Differentially expressed genes were identified using one-way ANOVA. For the analysis of *Sox9* cKO mice, sequencing libraries were prepared using the INCPM mRNA protocol. Reads were sequenced on an Illumina HiSeq 2500v4 SR60. Sequenced reads were mapped to the *Mus musculus* genome version GRCm38, using TopHat v2.0.10. Genes were identified using a .gtf obtained from Ensembl release 82. Per gene reads were counted using HTSeq. Normalization of read counts and *P*-values for differentially expressed genes were computed using DESeq2. *P*-values were adjusted for multiple testing using Benjamini–Hochberg FDR correction. For a gene to be considered differentially expressed (Table S1), we required a complete separation of expression levels between the two compared conditions (that is, we required the minimum level measured for the gene in one condition to be at least 20% higher than the maximum level measured for the same gene in the other condition).

Statistical analyses

Data obtained in qPCR experiments, CapMan analyses and quantifications by ImageJ (National Institutes of Health) were examined using two-tailed Student's *t*-test. *P*-values are indicated as $*P<0.05$, $**P<0.01$ and $***P<0.005$.

qPCR

Complementary DNA (cDNA) was amplified and analyzed as reported previously (Raviv et al., 2014). Each amplification reaction was performed in triplicate using 25 ng cDNA for each sample. Results were normalized to the house-keeping gene *Tbp*, after verifying that levels were comparable in normal and mutant RPE. Primers are listed in Table S11.

Chromatin immunoprecipitation and immunoblotting

Chromatin immunoprecipitation (ChIP) was conducted as previously described (Sailaja et al., 2012) on differentiated hES-RPE cells grown as documented (Idelson et al., 2009). For each assay, 10^7 cells were used and immunoprecipitated with 4 µg of either rabbit anti-Pax6 (Covance, PRB-278) or rabbit anti-Sox9 (Millipore, AB5535). ChIP-seq libraries were prepared and sequenced as previously described (Bramswig et al., 2013). The primers used for ChIP analysis by qPCR are listed in Table S11.

SOX9 ChIP-seq analysis

For ChIP-seq data [Gene Expression Omnibus (GEO) accession number GSE114305] analysis, sequenced reads were mapped to the human genome (v19) using bowtie2 (Langmead et al., 2009) (see Table S9 for alignment statistics). SOX9 binding sites ('peaks') were called using MACS2 (Zhang et al., 2008). Only uniquely mapped reads were used for peak calling. Motif enrichment analysis was done using DREME (Bailey, 2011).

Development (2018) 145, dev163691. doi:10.1242/dev.163691

Fluorescence quantification and cell counting

VE-Cad, Pax6 and Sox9 fluorescence intensity was quantified automatically using ImageJ software, and by multiplying the area of positive staining by the mean intensity, normalized to the background intensity in each individual image. The intensity was normalized by calculating the ratio between the differences of the mean intensity and the minimum and maximum intensities in each image. Quantification of the vascular area by IsoB4 labeling was further normalized to eye diameter owing to differences in eye size between genotypes, because the *Pax6* cKO mice present with microphthalmia.

In vivo electroporation

Injection of pCAG-GFP and pCAG-Pax6-IRES-GFP vectors into the subretinal space of P0 mice was followed by electroporation according to the protocol described for the mouse retina (Matsuda and Cepko, 2004; Remez et al., 2017). Eyes were harvested at P4, and four electroporated eyes were examined for each genotype by immunofluorescence assays labeling for Pax6, Sox9 and GFP. Analysis involved automatically separating areas not labeled with either GFP or Pax6, and areas labeled for one of them according to the vector injected. The intensity of Sox9-labeled pixels in the nucleus in each image was quantified by ImageJ, and an average was calculated for the electroporated and unelectroporated cells to assess the fold change in gene expression.

FITC-labeled albumin perfusions and flatmount

Perfusions were conducted as described (Tsai et al., 2009). Mice were cooled in ice water for 15 min, with the heads down, and the eyes were dissected out and fixed overnight in 4% paraformaldehyde. Next, the RPE and choroid were carefully dissected out, flattened on slides, and sealed with a solution of 0.05% azide, 60% sucrose and 1% agarose in PBS. Imaging was performed using confocal Leica STED microscopy to create *z*-stacks.

Classification and quantification of vascular layers

Boosted decision tree

The method of choice for this classification was boosted decision tree (BDT) (Freund et al., 1996). A decision tree is a binary tree structured classifier. A single decision tree is trained on a sample of known composition and tested on an independent known sample. All provided variables are scanned at each step to find the single cut that best separates signal from background according to a chosen metric. The sample is divided by the chosen cut, and the algorithm is applied again on each resulting subsample. This sample splitting continues until a stopping condition is reached, usually the minimum number of events allowed in a subsample (minimum leaf size). Hence, a single decision tree makes a series of cuts, but does not discard events: an event which fails a given cut continues to be considered by the algorithm. The algorithm divides up the space into signal-like and background-like regions, and assigns a score to each event depending on the appropriate region.

'Boosting' is a common method to improve the performance and stability of decision trees. After the first tree is trained, events are weighted such that those misclassified by the first tree have their weights increased. A second tree is then trained on this re-weighted sample, which naturally focuses on the events that were problematic in the first tree. This is a single 'boost'. The number of boosts must be optimized. At the end of the boosting cycle, a score is assigned to each event using a weighted average of the score calculated in each tree. The weight used is derived from the misclassification rate of each tree.

Preprocessing and feature extraction

A BDT makes use of a set of discriminating variables. Owing to the nature of the problem, the analysis in this study considered four features, which are described below:

(1) Intensity: the raw intensity of the pixel as recorded by the confocal microscope's camera (Fig. S5A).

(2, 3) Oriented maximum distance and oriented minimum distance: to obtain an estimation of the vessel diameter and length, a search for neighboring background pixel is performed in two opposite directions. When a background pixel is reached, the distance between the source and background pixels is measured. The longest distance is defined as the maximum and the shortest is the minimum. Prior to each step, a certain level of randomness is applied to direction selection in order to account for nonlinearity in vessels. At each step, there is a 35% chance of choosing a new direction (of a possible 16) to advance and a 65% chance of pursuing the original direction. A threshold of one background pixel was chosen (Fig. S5C,D) as a compromise between sensitivity and image noise.

(4) Maximum random step: similar to the oriented distances, this feature makes five attempts to count the number of steps (pixels advanced) before encountering background pixels. Advancing from the original pixel, each step direction is chosen randomly without reference to previous one. Larger, thicker vessels have a higher value because the 'walk' can continue longer (Fig. S5B).

Each feature was smoothed using the values of the neighbor pixels averaged with a 2D Gaussian function with a variance of five pixels as a weight. This gives a pixel feature value as:

$$\theta(x,y) = \frac{1}{N}\sum_{i}^{N}\left[\theta(x_i,y_i)e^{-\frac{(x-x_i)^2}{2\sigma^2}-\frac{(y-y_i)^2}{2\sigma^2}}\right].$$

Training and testing sets

Four sample images were produced by staining the larger vessels and CC separately in Photoshop, providing 3.5×10^6 events for training and testing the BDT. These images were not used in the final analysis. The training was performed using a Toolkit for Multivariate Data Analysis (TMVA) (Hoecker et al., 2007 preprint). The samples were divided so that half were used for training and the rest for testing of the model. Evaluation of the BDT on both the training and testing sample (Fig. S5H, signal representing CC and background representing A&V) compared with values obtained with each of the four features separately (Fig. S5G), demonstrated an accuracy of 0.877.

Cutting on BDT output

The preprocessing of each image creates the discussed four features on which the BDT is applied. The BDT output gives each pixel a score between −1 and +1, describing the probability of that pixel being part of a larger vessel or the capillary network. Based on the training, the threshold in this scale that achieved the maximal number of true positives was automatically determined by BDT as 0.

Acknowledgements

We thank Haruhiko Akiyama, Kyoto University, and Eli Zelzer, Weizmann Institute of Science, for providing the *Sox9*^{loxP} mice; Yuval Dor and Ahuvit David for help during revision; and Noriko Osumi, Johns Hopkins University, for reagents and advice.

Competing interests

The authors declare no competing or financial interests.

Author contributions

Conceptualization: Y.C.-T., H.C., R.E., R.A.-P.; Methodology: Y.C.-T., H.C., Y.M., Z.A., C.L., M.I., B.R., S.I., S.R., K.H.K. P.B., R.E., R.A.-P.; Software: H.C., R.E.; Validation: Y.C.-T., Z.A., R.E., R.A.-P.; Formal analysis: Y.C.-T., R.E., R.A.-P.; Investigation: Y.C.-T., P.B., Z.A., R.E., R.A.-P.; Resources: Y.C.-T. M.I., B.R., S.R., K.H.K. P.B., R.A.-P.; Data curation: Y.C.-T., H.C., R.E., R.A.-P.; Writing - original draft: Y.C.-T., R.E., R.A.-P.; Writing - review & editing: H.C., C.L., S.I., P.B., R.E., R.A.-P.; Visualization: Y.C.-T., Z.A., R.E., R.A.-P.; Supervision: P.B., B.R., S.I., R.E., R.A.-P.; Project administration: R.A.-P.; Funding acquisition: K.H.K., P.B., R.A.-P.

Funding

Research in the R.A.-P. laboratory is supported by grants from the Israel Science Foundation [228/14], the Israel National Center for Personalized Medicine (INCPM) Israel Science Foundation [2246/16], the Israel Science Foundation-National Natural Science Foundation of China joint research program [2469/16], and the United States-Israel Binational Science Foundation [2013016]. P.B. is supported by the Israel Science Foundation [1019/15] and by a grant from the Claire and Amedee Maratier Institute for the Study of Blindness and Visual Disorders, Sackler Faculty of Medicine, Tel-Aviv University, Israel.

Data availability

ChIP-seq data are available in GEO under accession number GSE114305. RNA-seq data are available in GEO under accession number GSE114945. The affymetrix microarray data for hES-RPE (d5, d14) are available in GEO under accession number GSE117709.

Supplementary information

Supplementary information available online at
http://dev.biologists.org/lookup/doi/10.1242/dev.163691.supplemental

References

Ahmad, Z., Rafeeq, M., Collombat, P. and Mansouri, A. (2015). Pax6 inactivation in the adult pancreas reveals ghrelin as endocrine cell maturation marker. *PLoS ONE* **10**, e0144597.

Akiyama, H., Chaboissier, M.-C., Martin, J. F., Schedl, A. and de Crombrugghe, B. (2002). The transcription factor Sox9 has essential roles in successive steps of the chondrocyte differentiation pathway and is required for expression of Sox5 and Sox6. *Genes Dev.* **16**, 2813-2828.

Ambati, B. K., Nozaki, M., Singh, N., Takeda, A., Jani, P. D., Suthar, T., Albuquerque, R. J. C., Richter, E., Sakurai, E., Newcomb, M. T. et al. (2006). Corneal avascularity is due to soluble VEGF receptor-1. *Nature* **443**, 993-997.

Amram, B., Cohen-Tayar, Y., David, A. and Ashery-Padan, R. (2017). The retinal pigmented epithelium – from basic developmental biology research to translational approaches. *Int. J. Dev. Biol.* **61**, 225-234.

Andrade, C. (1952). A peculiar form of peripheral neuropathy; familiar atypical generalized amyloidosis with special involvement of the peripheral nerves. *Brain* **75**, 408-427.

Ashery-Padan, R. (2000). Pax6 activity in the lens primordium is required for lens formation and for correct placement of a single retina in the eye. *Genes Dev.* **14**, 2701-2711.

Babapoor-Farrokhran, S., Jee, K., Puchner, B., Hassan, S. J., Xin, X., Rodrigues, M., Kashiwabuchi, F., Ma, T., Hu, K., Deshpande, M. et al. (2015). Angiopoietin-like 4 is a potent angiogenic factor and a novel therapeutic target for patients with proliferative diabetic retinopathy. *Proc. Natl. Acad. Sci. USA* **112**, E3030-E3039.

Bai, Y., Ma, J., Guo, J., Wang, J., Zhu, M., Chen, Y. and Le, Y.-Z. (2009). Müller cell-derived VEGF is a significant contributor to retinal neovascularization. *J. Pathol.* **219**, 446-454.

Bailey, T. L. (2011). DREME: motif discovery in transcription factor ChIP-seq data. *Bioinformatics* **27**, 1653-1659.

Bäumer, N., Marquardt, T., Stoykova, A., Spieler, D., Treichel, D., Ashery-Padan, R. and Gruss, P. (2003). Retinal pigmented epithelium determination requires the redundant activities of Pax2 and Pax6. *Development* **130**, 2903-2915.

Bhandari, R. K., Haque, M. M. and Skinner, M. K. (2012). Global genome analysis of the downstream binding targets of testis determining factor SRY and SOX9. *PLoS ONE* **7**, e43380.

Bharti, K., Gasper, M., Ou, J., Brucato, M., Clore-Gronenborn, K., Pickel, J. and Arnheiter, H. (2012). A regulatory loop involving PAX6, MITF, and WNT signaling controls retinal pigment epithelium development. *PLoS Genet.* **8**, e1002757.

Bhutto, I. and Lutty, G. (2012). Understanding age-related macular degeneration (AMD): relationships between the photoreceptor/retinal pigment epithelium/Bruch's membrane/choriocapillaris complex. *Mol. Aspects Med.* **33**, 295-317.

Blaauwgeers, H. G., Holtkamp, G. M., Rutten, H., Witmer, A. N., Koolwijk, P., Partanen, T. A., Alitalo, K., Kroon, M. E., Kijlstra, A., van Hinsbergh, V. W. et al. (1999). Polarized vascular endothelial growth factor secretion by human retinal pigment epithelium and localization of vascular endothelial growth factor receptors on the inner choriocapillaris. Evidence for a trophic paracrine relation. *Am. J. Pathol.* **155**, 421-428.

Bramswig, N. C., Everett, L. J., Schug, J., Dorrell, C., Liu, C., Luo, Y., Streeter, P. R., Naji, A., Grompe, M. and Kaestner, K. H. (2013). Epigenomic plasticity enables human pancreatic α to β cell reprogramming. *J. Clin. Invest.* **123**, 1275-1284.

Carpenter, A. C., Smith, A. N., Wagner, H., Cohen-Tayar, Y., Rao, S., Wallace, V., Ashery-Padan, R. and Lang, R. A. (2015). Wnt ligands from the embryonic surface ectoderm regulate "bimetallic strip" optic cup morphogenesis in mouse. *Development* **142**, 972-982.

Cook, J., Radu, R., Sun, H. and Travis, G. (2013). Functional characterization of peropsin in the retinal pigment epithelium. *Invest. Ophthalmol. Vis. Sci.* **54**, 3764.

Cooper, G. M., Stone, E. A., Asimenos, G., NISC Comparative Sequencing Program, Green, E. D., Batzoglou, S. and Sidow, A. (2005). Distribution and intensity of constraint in mammalian genomic sequence. *Genome Res.* **15**, 901-913.

Davis, N., Yoffe, C., Raviv, S., Antes, R., Berger, J., Holzmann, S., Stoykova, A., Overbeek, P. A., Tamm, E. R. and Ashery-Padan, R. (2009). Pax6 dosage requirements in iris and ciliary body differentiation. *Dev. Biol.* **333**, 132-142.

Defoe, D. M. and Levine, E. M. (2003) Expression of the cyclin-dependent kinase inhibitor p27Kip1 by developing retinal pigment epithelium. *Gene Expr. Patt.* **3**, 615-619.

Dwork, A. J., Cavallaro, T., Martone, R. L., Goodman, D. S., Schon, E. A. and Herbert, J. (1990). Distribution of transthyretin in the rat eye. *Invest. Ophthalmol. Vis. Sci.* **31**, 489-496.

Eshkar-Oren, I., Viukov, S. V., Salameh, S., Krief, S., Oh, C., Akiyama, H., Gerber, H.-P., Ferrara, N. and Zelzer, E. (2009). The forming limb skeleton serves as a signaling center for limb vasculature patterning via regulation of Vegf. *Development* **136**, 1263-1272.

Freund, Y. and Schapire, R. E. (1996). Experiments with a new boosting algorithm. *Proc. Thirteen. Int. Conf. Mach. Learn.* 148-156. Morgan Kaufmann Publishers: San Francisco, CA. dl.acm.org/citation.cfm?id=3091715.

Fryczkowski, A. W. (1994). Anatomical and functional choroidal lobuli. *Int. Ophthalmol.* **18**, 131-141.

Goodwin, A. M. (2007). In vitro assays of angiogenesis for assessment of angiogenic and anti-angiogenic agents. *Microvasc. Res.* **74**, 172-183.

Goto, S., Onishi, A., Misaki, K., Yonemura, S., Sugita, S., Ito, H., Ohigashi, Y., Ema, M., Sakaguchi, H., Nishida, K. et al. (2018). Neural retina-specific Aldh1a1 controls dorsal choroidal vascular development via Sox9 expression in retinal pigment epithelial cells. *elife* **7**, e32358.

Hageman, G. S., Luthert, P. J., Chong, N. H. V., Johnson, L. V., Anderson, D. H. and Mullins, R. F. (2001). An integrated hypothesis that considers Drusen as biomarkers of immune-mediated processes at the RPE-Bruch's membrane interface in aging and age-related macular degeneration. **20**, 705-732.

Hägglund, A.-C., Berghard, A. and Carlsson, L. (2013). Canonical Wnt/β-catenin signalling is essential for optic cup formation. *PLoS ONE* **8**, e81158.

Hart, A. W., Mella, S., Mendrychowski, J., van Heyningen, V. and Kleinjan, D. A. (2013). The developmental regulator Pax6 is essential for maintenance of islet cell function in the adult mouse pancreas. *PLoS ONE* **8**, e54173.

Hayreh, S. S. (1975). Segmental nature of the choroidal vasculature. *Br. J. Ophthalmol.* **59**, 631-648.

Herbert, J., Wilcox, J. N., Pham, K. T., Fremeau, R. T., Zeviani, M., Dwork, A., Soprano, D. R., Makover, A., Goodman, D. S., Zimmerman, E. A. et al. (1986). Transthyretin: a choroid plexus-specific transport protein in human brain. The 1986 S. Weir Mitchell award. *Neurology* **36**, 900-911.

Hingorani, M., Hanson, I. and van Heyningen, V. (2012). Aniridia. *Eur. J. Hum. Genet.* **20**, 1011-1017.

Hoecker, A., Speckmayer, P., Stelzer, J., Therhaag, J., von Toerne, E., Voss, H. (2007). TMVA - Toolkit for Multivariate Data Analysis. PoS ACAT 040, *arXiv*: physics/0703039.

Huang, D. W., Sherman, B. T. and Lempicki, R. A. (2009). Systematic and integrative analysis of large gene lists using DAVID bioinformatics resources. *Nat. Protoc.* **4**, 44-57.

Huang, R.-L., Teo, Z., Chong, H. C., Zhu, P., Tan, M. J., Tan, C. K., Lam, C. R. I., Sng, M. K., Leong, D. T. W., Tan, S. M. et al. (2011). ANGPTL4 modulates vascular junction integrity by integrin signaling and disruption of intercellular VE-cadherin and claudin-5 clusters. *Blood* **118**, 3990-4002.

Idelson, M., Alper, R., Obolensky, A., Ben-Shushan, E., Hemo, I., Yachimovich-Cohen, N., Khaner, H., Smith, Y., Wiser, O., Gropp, M. et al. (2009). Directed differentiation of human embryonic stem cells into functional retinal pigment epithelium cells. *Cell Stem Cell* **5**, 396-408.

Kadaja, M., Keyes, B. E., Lin, M., Pasolli, H. A., Genander, M., Polak, L., Stokes, N., Zheng, D. and Fuchs, E. (2014). SOX9: a stem cell transcriptional regulator of secreted niche signaling factors. *Genes Dev.* **28**, 328-341.

Kamachi, Y. and Kondoh, H. (2013). Sox proteins: regulators of cell fate specification and differentiation. *Development* **140**, 4129-4144.

Kamachi, Y., Uchikawa, M., Tanouchi, A., Sekido, R. and Kondoh, H. (2001). Pax6 and SOX2 form a co-DNA-binding partner complex that regulates initiation of lens development. *Genes Dev.* **15**, 1272-1286.

Klimova, L. and Kozmik, Z. (2014). Stage-dependent requirement of neuroretinal Pax6 for lens and retina development. *Development* **141**, 1292-1302.

Kondoh, H. and Kamachi, Y. (2010). SOX–partner code for cell specification: regulatory target selection and underlying molecular mechanisms. *Int. J. Biochem. Cell Biol.* **42**, 391-399.

Korte, G. E., Reppucci, V. and Henkind, P. (1984). RPE destruction causes choriocapillary atrophy. *Investig. Ophthalmol. Vis. Sci.* **25**, 1135-1145.

Kurihara, T. (2016). Development and pathological changes of neurovascular unit regulated by hypoxia response in the retina. *Prog. Brain Res.* **225**, 201-211.

Langmead, B., Trapnell, C., Pop, M. and Salzberg, S. L. (2009). Ultrafast and memory-efficient alignment of short DNA sequences to the human genome. *Genome Biol.* **10**, R25.

Lee, H. J. and Colby, K. A. (2013). A review of the clinical and genetic aspects of aniridia. *Semin. Ophthalmol.* **28**, 306-312.

Liao, J.-L., Yu, J., Huang, K., Hu, J., Diemer, T., Ma, Z., Dvash, T., Yang, X.-J., Travis, G. H., Williams, D. S. et al. (2010). Molecular signature of primary retinal pigment epithelium and stem-cell-derived RPE cells. *Hum. Mol. Genet.* **19**, 4229-4238.

Lutty, G. A., Hasegawa, T., Baba, T., Grebe, R., Bhutto, I. and McLeod, D. S. (2010). Development of the human choriocapillaris. *Eye* **24**, 408-415.

Lyubimova, A., Itzkovitz, S., Junker, J. P., Fan, Z. P., Wu, X. and van Oudenaarden, A. (2013). Single-molecule mRNA detection and counting in mammalian tissue. *Nat. Protoc.* **8**, 1743-1758.

Marneros, A. G., Fan, J., Yokoyama, Y., Gerber, H. P., Ferrara, N., Crouch, R. K. and Olsen, B. R. (2005). Vascular endothelial growth factor expression in the retinal pigment epithelium is essential for choriocapillaris development and visual function. *Am. J. Pathol.* **167**, 1451-1459.
Masuda, T. and Esumi, N. (2010). SOX9, through interaction with microphthalmia-associated transcription factor (MITF) and OTX2, regulates BEST1 expression in the retinal pigment epithelium. *J. Biol. Chem.* **285**, 26933-26944.
Masuda, T., Wahlin, K., Wan, J., Hu, J., Maruotti, J., Yang, X., Iacovelli, J., Wolkow, N., Kist, R., Dunaief, J. L. et al. (2014). Transcription factor SOX9 plays a key role in the regulation of visual cycle gene expression in the retinal pigment epithelium. *J. Biol. Chem.* **289**, 12908-12921.
Matsuda, T. and Cepko, C. L. (2004). Electroporation and RNA interference in the rodent retina in vivo and in vitro. *Proc. Natl. Acad. Sci. USA* **101**, 16-22.
Matsushima, D., Heavner, W. and Pevny, L. H. (2011). Combinatorial regulation of optic cup progenitor cell fate by SOX2 and PAX6. *Development* **138**, 443-454.
Mertin, S., McDowall, S. G. and Harley, V. R. (1999). The DNA-binding specificity of SOX9 and other SOX proteins. *Nucleic Acids Res.* **27**, 1359-1364.
Mirzayans, F., Pearce, W. G., MacDonald, I. M. and Walter, M. A. (1995). Mutation of the PAX6 gene in patients with autosomal dominant keratitis. *Am. J. Hum. Genet.* **57**, 539-548.
Newman, A. M., Gallo, N. B., Hancox, L. S., Miller, N. J., Radeke, C. M., Maloney, M. A., Cooper, J. B., Hageman, G. S., Anderson, D. H., Johnson, L. V. et al. (2012). Systems-level analysis of age-related macular degeneration reveals global biomarkers and phenotype-specific functional networks. *Genome Med.* **4**, 16.
Nickla, D. L. and Wallman, J. (2010). The multifunctional choroid. *Prog. Retin. Eye Res.* **29**, 144-168.
Nunes, R. J., de Oliveira, P., Lages, A., Becker, J. D., Marcelino, P., Barroso, E., Perdigoto, R., Kelly, J. W., Quintas, A. and Santos, S. C. R. (2013). Transthyretin proteins regulate angiogenesis by conferring different molecular identities to endothelial cells. *J. Biol. Chem.* **288**, 31752-31760.
Oh, C., Maity, S. N., Lu, J.-F., Zhang, J., Liang, S., Coustry, F., de Crombrugghe, B. and Yasuda, H. (2010). Identification of SOX9 interaction sites in the genome of chondrocytes. *PLoS ONE* **5**, e10113.
Okabe, K., Kobayashi, S., Yamada, T., Kurihara, T., Tai-Nagara, I., Miyamoto, T., Mukouyama, Y., Sato, T. N., Suda, T., Ema, M. et al. (2014). Neurons limit angiogenesis by titrating VEGF in retina. *Cell* **159**, 584-596.
Oron-Karni, V., Farhy, C., Elgart, M., Marquardt, T., Remizova, L., Yaron, O., Xie, Q., Cvekl, A. and Ashery-Padan, R. (2008). Dual requirement for Pax6 in retinal progenitor cells. *Development* **135**, 4037-4047.
Philips, G. T., Stair, C. N., Young Lee, H., Wroblewski, E., Berberoglu, M. A., Brown, N. L. and Mastick, G. S. (2005). Precocious retinal neurons: Pax6 controls timing of differentiation and determination of cell type. *Dev. Biol.* **279**, 308-321.
Poché, R. A., Furuta, Y., Chaboissier, M.-C., Schedl, A. and Behringer, R. R. (2008). Sox9 is expressed in mouse multipotent retinal progenitor cells and functions in Müller glial cell development. *J. Comp. Neurol.* **510**, 237-250.
Raviv, S., Bharti, K., Rencus-Lazar, S., Cohen-Tayar, Y., Schyr, R., Evantal, N., Meshorer, E., Zilberberg, A., Idelson, M., Reubinoff, B. et al. (2014). PAX6 regulates melanogenesis in the retinal pigmented epithelium through feed-forward regulatory interactions with MITF. *PLoS Genet.* **10**, e1004360.
Remez, L. A., Onishi, A., Menuchin-Lasowski, Y., Biran, A., Blackshaw, S., Wahlin, K. J., Zack, D. J. and Ashery-Padan, R. (2017). Pax6 is essential for the generation of late-born retinal neurons and for inhibition of photoreceptor-fate during late stages of retinogenesis. *Dev. Biol.* **432**, 140-150.
Reubinoff, B. E., Pera, M. F., Fong, C.-Y., Trounson, A. and Bongso, A. (2000). Embryonic stem cell lines from human blastocysts: somatic differentiation in vitro. *Nat. Biotechnol.* **18**, 399-404.
Sailaja, B. S., Takizawa, T. and Meshorer, E. (2012). Chromatin immunoprecipitation in mouse hippocampal cells and tissues. *Methods Mol. Biol.* **809**, 353-364.
Saint-Geniez, M. and D'Amore, P. A. (2004). Development and pathology of the hyaloid, choroidal and retinal vasculature. *Int. J. Dev. Biol.* **48**, 1045-1058.
Saint-Geniez, M., Maldonado, A. E. and D'Amore, P. A. (2006). VEGF expression and receptor activation in the choroid during development and in the adult. *Invest. Ophthalmol. Vis. Sci.* **47**, 3135-3142.
Saint-Geniez, M., Kurihara, T., Sekiyama, E., Maldonado, A. E. and D'Amore, P. A. (2009). An essential role for RPE-derived soluble VEGF in the maintenance of the choriocapillaris. *Proc. Natl. Acad. Sci. USA* **106**, 18751-18756.
Sakamoto, T., Sakamoto, H., Murphy, T. L., Spee, C., Soriano, D., Ishibashi, T., Hinton, D. R. and Ryan, S. J. (1995). Vessel formation by choroidal endothelial cells in vitro is modulated by retinal pigment epithelial cells. *Arch. Ophthalmol.* **113**, 512-520.
Sellheyer, K. (1990). Development of the choroid and related structures. *Eye* **4**, 255-261.
Shaham, O., Smith, A. N., Robinson, M. L., Taketo, M. M., Lang, R. A. and Ashery-Padan, R. (2009). Pax6 is essential for lens fiber cell differentiation. *Development* **136**, 2567-2578.
Shaham, O., Gueta, K., Mor, E., Oren-Giladi, P., Grinberg, D., Xie, Q., Cvekl, A., Shomron, N., Davis, N., Keydar-Prizant, M. et al. (2013). Pax6 regulates gene expression in the vertebrate lens through miR-204. *PLoS Genet.* **9**, e1003357.
Shi, Z., Chiang, C.-I., Labhart, P., Zhao, Y., Yang, J., Mistretta, T.-A., Henning, S. J., Maity, S. N. and Mori-Akiyama, Y. (2015). Context-specific role of SOX9 in NF-Y mediated gene regulation in colorectal cancer cells. *Nucleic Acids Res.* **43**, 6257-6269.
Smith, A. N., Miller, L.-A., Radice, G., Ashery-Padan, R. and Lang, R. A. (2009). Stage-dependent modes of Pax6-Sox2 epistasis regulate lens development and eye morphogenesis. *Development* **136**, 2977-2985.
Sodhi, A. and Montaner, S. (2015). Angiopoietin-like 4 as an emerging therapeutic target for diabetic eye disease. *JAMA Ophthalmol.* **133**, 1375-1376.
Song, M. J. and Bharti, K. (2016). Looking into the future: using induced pluripotent stem cells to build two and three dimensional ocular tissue for cell therapy and disease modeling. *Brain Res.* **1638**, 2-14.
Songstad, A. E., Wiley, L. A., Duong, K., Kaalberg, E., Flamme-Wiese, M. J., Cranston, C. M., Riker, M. J., Levasseur, D., Stone, E. M., Mullins, R. F. et al. (2015). Generating iPSC-derived choroidal endothelial cells to study age-related macular degeneration. *Investig. Opthalmol. Vis. Sci.* **56**, 8258.
Spilsbury, K., Garrett, K. and Shen, W. (2000). Overexpression of vascular endothelial growth factor (VEGF) in the retinal pigment epithelium leads to the development of choroidal neovascularization. *Am. J.* **157**, 135-144.
Strauss, O. (2005). The retinal pigment epithelium in visual function. *Physiol. Rev.* **85**, 845-881.
Swisa, A., Avrahami, D., Eden, N., Zhang, J., Feleke, E., Dahan, T., Cohen-Tayar, Y., Stolovich-Rain, M., Kaestner, K. H., Glaser, B. et al. (2016). PAX6 maintains β cell identity by repressing genes of alternative islet cell types. *J. Clin. Invest.* **127**, 230-243.
Tan, M. J., Teo, Z., Sng, M. K., Zhu, P. and Tan, N. S. (2012). Emerging roles of angiopoietin-like 4 in human cancer. *Mol. Cancer Res.* **10**, 677-688.
Ton, C. C. T., Hirvonen, H., Miwa, H., Weil, M. M., Monaghan, P., Jordan, T., van Heyningen, V., Hastie, N. D., Meijers-Heijboer, H., Drechsler, M. et al. (1991). Positional cloning and characterization of a paired box- and homeobox-containing gene from the aniridia region. *Cell* **67**, 1059-1074.
Tsai, P. S., Kaufhold, J. P., Blinder, P., Friedman, B., Drew, P. J., Karten, H. J., Lyden, P. D. and Kleinfeld, D. (2009). Correlations of neuronal and microvascular densities in murine cortex revealed by direct counting and colocalization of nuclei and vessels. *J. Neurosci.* **29**, 14553-14570.
Tusher, V. G., Tibshirani, R. and Chu, G. (2001). Significance analysis of microarrays applied to the ionizing radiation response. *Proc. Natl. Acad. Sci. USA* **98**, 5116-5121.
Wang, Q., Chen, Q., Zhao, K., Wang, L., Wang, L. and Traboulsi, E. I. (2001). Update on the molecular genetics of retinitis pigmentosa. *Ophthalmic Genet.* **22**, 133-154.
Zhang, Y., Liu, T., Meyer, C. A., Eeckhoute, J., Johnson, D. S., Bernstein, B. E., Nussbaum, C., Myers, R. M., Brown, M., Li, W. et al. (2008). Model-based analysis of ChIP-Seq (MACS). *Genome Biol.* **9**, R137.
Zhao, S. and Overbeek, P. A. (2001). Regulation of choroid development by the retinal pigment epithelium. *Mol. Vis.* **7**, 277-282.
Zhou, Y.-H., Hu, Y., Mayes, D., Siegel, E., Kim, J. G., Mathews, M. S., Hsu, N., Eskander, D., Yu, O., Tromberg, B. J. et al. (2010). PAX6 suppression of glioma angiogenesis and the expression of vascular endothelial growth factor A. *J. Neurooncol.* **96**, 191-200.
Zurdel, J., Zubaty, V., Nitsch, R. and Richard, G. (2002a). Immunohistochemical analysis of Cystatin C in age-related macular degeneration. *Invest. Ophthalmol. Vis. Sci.* **43**, 2783.
Zurdel, J., Finckh, U., Menzer, G., Nitsch, R. M. and Richard, G. (2002b). CST3 genotype associated with exudative age related macular degeneration. *Br. J. Ophthalmol.* **86**, 214-219.